Journal of Power Sources 195 (2010) 7207–7212

Contents lists available at ScienceDirect

Journal of Power Sources

journal homepage: www.elsevier.com/locate/jpowsour

Synthesis and characterization of $Bi_{31}Cr_5O_{61.5}$, a new bismuth chromium oxide, potential mixed-ionic–electronic conductor for solid oxide fuel cells

Marie Colmont*, Michel Drache, Pascal Roussel

Université Lille Nord de France, Unité de Catalyse et de Chimie du Solide (UCCS), CNRS UMR 8181, 59655 Villeneuve d'Ascq Cedex, France

ARTICLE INFO

Article history:
Received 4 March 2010
Received in revised form 29 April 2010
Accepted 9 May 2010
Available online 9 June 2010

Keywords:
Bismuth chromium oxide
Fluorite type structure
Single crystal structure refinement
Electrical conductivity properties

ABSTRACT

Single crystals, as well as pure powder of the new bismuth chromate, $Bi_{31}Cr_5O_{61.5}$ were synthesized by slow cooling of a mixture of Bi_2O_3–Cr_2O_3 and then fully structurally characterized using X-ray diffraction. It crystallizes in the monoclinic space group $P2_1/n$ with unit cell parameters $a = 23.5794(8)$, $b = 11.6189(4)$, $c = 24.3629(8)$ Å and $\beta = 108.02(1)^\circ$, $Z = 4$. The final conventional agreement factors converged to $R = 0.0540$ and $wR = 0.0561$ for 27520 independent reflections. The +VI chromium oxidation state was proved by thermogravimetric and magnetic measurements. The structure can be described by the association of isolated CrO_4 tetrahedra surrounded by 11 or 12 Bi atoms forming truncated or not cuboctahedra. The stability of both pure powder sample and pressed sintered pellets was studied at elevated temperature by X-ray diffraction and by dilatometry previously to ionic conductivity measurements done by impedance spectroscopy.

1. Introduction

The δ-Bi_2O_3 phase has seen many interests these last decades as material for solid oxide fuel cells (SOFCs) since it is the best oxide anion conductor at high temperature [1]. Nevertheless, the phase stability domain is very small and the α-Bi_2O_3 polymorph is the only one stable at room temperature [2]. The goal to reach might be to synthesize a structurally related phase with such interesting conducting properties but with a lower temperature of use. Until now, many δ-related phases have been stabilized at room temperature but their conductivity performances are unfortunately poorer than expected [3–8]. This is essentially due to the oxygen ordering of the oxygen network while the interesting conductivity property in δ-Bi_2O_3 has been associated to the defective and disorder characters of the oxide sub-lattice [9]. The oxide mobility appears to be linked to the polarizability of cationic sub-network. Consequently, the higher the bismuth content, the better is the materials conductivity. The idea underlying is to try to substitute Bi by a cation to stabilize the δ conducting phase at lower temperature, keeping thus a high rate of bismuth [10,11].

The binary system Bi_2O_3–Cr_2O_3 has been largely investigated leading to numerous phases [12–14] of which three are closely related to the fluorite structure: $Bi_{14}CrO_{24}$ [10], $Bi_6Cr_2O_{15}$ [15] and $Bi_{1-x}Cr_xO_{1.5+1.5x'}$, $0.05 \leq x \leq 0.15$ [16].

New investigations reported in this paper were realized with the aim of determining a new bismuth chromium material which might be potentially ionic and electronic conductor, namely a so called MIEC, acronym for mixed-ionic–electronic conductor. Indeed, beside the ionic conductivity expected for the δ-Bi_2O_3 network, the ability of chromium to change its oxidation state from 6 to 5 or 4 can lead to electronic conductivity and hence to a potential MIEC.

In the present manuscript, the new $Bi_{31}Cr_5O_{61.5}$ compound has been synthesized and its crystal structure was determined and related to the δ-Bi_2O_3 phase. Preliminary conductivity performances have been tested.

2. Experimental section

2.1. Single crystal growth

Single crystals of the new title-phase have been obtained from the slow cooling (5 °C h^{-1}) of a mixture of Bi_2O_3 (Aldrich, 99.9%) and Cr_2O_3 (Prolabo, 99.00%) in ratio 3:1:1 after melting it in a gold boat at 850 °C. Orange needle shaped crystals corresponding to the new $Bi_{31}Cr_5O_{61.5}$ were extracted of the homogeneous melt. The selection of good quality crystals was based upon the sharpness of the diffraction spots. The conditions of data collection are summarized in Table 1.

2.2. Powder synthesis

$Bi_{31}Cr_5O_{61.5}$ powder sample was afterward prepared by solid state reaction. Bi_2O_3 (Aldrich, 99.9%) and Cr_2O_3 (Prolabo, 99.00%)

* Corresponding author. Tel.: +33 0320 436 434; fax: +33 0320 436 561.
E-mail address: marie.colmont@ensc-lille.fr (M. Colmont).

0378-7753/$ – see front matter © 2010 Elsevier B.V. All rights reserved.
doi:10.1016/j.jpowsour.2010.05.013

Table 1
Crystal data and structure refinements for $Bi_{31}Cr_5O_{61.5}$.

Crystallographic data	
Nominal formula	$Bi_{31}Cr_5O_{61.5}$
Refined formula	$Bi_{31}Cr_5O_{59}$
Symmetry	Monoclinic
Space group	$P2_1/n$
Cell parameters (Å)	$a = 23.5794$ $b = 11.6189$ $c = 24.3629$ $\beta = 108.03$
Cell volume (Å^3)	6346.9
Z	4
Density calculated (g cm^{-3})	8.04
F000	12660
Intensity collection	
2θ range (°)	1.76–34.94
Data collected	$-37 \le h \le 35$ $-16 \le k \le 18$ $-23 \le l \le 39$
No. of reflections collected	88912
No. of reflections measured	27520
No. of independent ($I > 3\sigma(I)$)	20000
Redundancy	3.23
Completeness (%/2θ (°))	99/69.8
μ_1 (Mo Kα) (mm^{-1})	92.367
T_{min}/T_{max} ratio	0.0146
$R(F^2)_{int}$	0.1525
Refinement	
No. of parameters	486
Weighting scheme	$1/\sigma^2$
$R(F)$ obs/all	0.0540/0.1854
w$R(F)$ obs/all	0.0561/0.0706
ρ_{max}, ρ_{min} (e Å^{-3})	3.61/−5.17

were used as started materials and introduced with the corresponding stoichiometric amounts. The reagents were weighed, placed in an agate mortar, closely grinded and homogenised. Then the sample was deposited in an alumina crucible and heated at 500 °C for 12 h and 800 °C during 24 h. The treatment ended by an air quenching.

2.3. TGA analysis

In order to determine the oxidation state of chromium, thermal analyses were performed under air in platinum crucibles on TG-DT 92-16.18 Setaram apparatus (heating and cooling rate 5 °C min^{-1}), between room temperature and 800 °C.

2.4. Elemental analysis

The EDS (energy dispersive spectroscopy) analysis was performed using a scanning electron microscope (JEOL JSM-5300 microscope) equipped with an energy dispersive spectrometer.

2.5. Magnetism

To evaluate precise oxidation state of chromium atoms in the structure, susceptibility measurements were measured from 300 to 4 K on a Quantum Design SQUID under an applied field of 2500 Gauss on 120 mg of compound.

2.6. Single crystal X-ray diffraction

A Bruker X8 Apex 2 CCD 4 K diffractometer equipped with a fine-focus Mo-target X-ray tube ($\lambda = 0.71073$ Å) was used for the crystallographic characterization of single crystals. A combination of phi and omega scans was used at a crystal-detector distance of 45 mm. Lorentz, polarisation and absorption effects were corrected with the Bruker Suite.

2.7. High-temperature X-ray diffraction (HTXRD)

In order to evaluate the temperature stability of the compound, HTXRD was performed on a Bruker axs D8 Advance diffractometer equipped with a high-temperature Anton Paar HTK 1200 N chamber and a one-dimensional X-ray detector (VÅNTEC-1) using Cu Kα radiation. Data were collected over the range 6–60° in 2θ, with a 0.015° step and a time of 0.2 s per step from room temperature to 850 °C. Diffractograms were obtained every 25 °C on heating and 100 °C cooling. Samples were deposited on platinum sheets to avoid any contamination with the alumina crucible.

2.8. Dilatometry analysis

Thermal expansion material investigation of sintered pellets (800 °C) was conducted under air using a Linseis L75 dilatometer (heating–cooling rate of 5 °C min^{-1} between room temperature and 800 °C.

2.9. Impedance spectroscopy measurement

In order to investigate the electrical conductivity properties, pellets (diameter ca 5 mm and thickness 3–4 mm) sintered at 800 °C, were elaborated from the material. The relative density determined from mass and dimensions of pellets and theoretical volume-mass of the material, was close to 85% for the different pellets tested. Impedance spectroscopy measurements were performed using a Solartron, SI 1260 analyzer in the 1.0 Hz to 1.0 MHz domain. The imposed signal amplitude during measurements was verified to be low enough (50 mV) for a zero DC polarization current approximation, with respect to the linearity of the electrical response. Gold electrodes were used as current collectors. Measurements were performed in air at various temperatures from 250 to 850 °C (temperature step 20 °C). Before each measurement it was checked that the electrochemical response was stable. Each set of values was recorded after 1 h stabilization range.

3. Structural investigation

In the collected data set, a lot of reflections with low intensity close to reflections of high intensity (related to the δ-Bi_2O_3 fluorine cubic subcell) were observed, suggesting a modulated structure, as observed in Ref. [16]. Nevertheless, all our attempts to determine the modulation vector were unsuccessful. The crystal structure was then treated as a "classical" superstructure, solved in the large unit cell using the SuperFlip [17] software, and refined with the JANA2006 [18] crystallographic suite. After absorption correction, the 27520 reflections ($I > 3\sigma(I)$) were merged in the Laue group $2/m$ leading to merging factor $R_{int} = 9.18\%$ for 7515 reflections with $I > 3\sigma(I)$. The refined monoclinic lattice parameters are: $a = 23.5794(8)$ Å, $b = 11.6189(4)$ Å, $c = 24.3629(8)$ Å and $\beta = 108.03(1)°$. The structural refinement satisfactory converges in the space group $P2_1/n$ which is compatible with the systematic observed absences.

Thirty-one independent heavy atoms of bismuth, 54 atoms of oxygen and 5 chromium atoms have been located. The Bi/Cr ratio has been confirmed by an elemental analysis performed on a scanning electron microscope by EDS. At this step, the single crystal refinement (refined formula: $Bi_{31}Cr_5O_{60}$) indicates an average oxidation state of 5.4 for chromium atom, and consequently a possible mixture of $Cr^{IV}/Cr^{V}/Cr^{VI}$ states. However, it is well known that the Cr^{V} oxidation state is not so common in oxides, even unstable, and

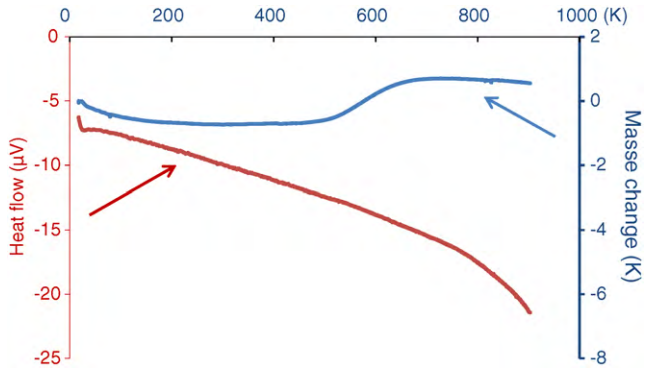

Fig. 1. DT-TG analysis of (31 Bi_2O_3–5 Cr_2O_3) stoechiometric mixture. The weight loss is representative of a chromium valence state of +5.85.

needs special complex synthesis conditions to be stabilized, which is not the case here. Cr^{IV} is a little more stable but not so common. To discriminate between the more probable +VI valence state and the exotic +IV or +V ones (difficult to determine by the X-ray refinement, which is not the best tool to observe "light" oxygen atoms near "heavy" bismuth atoms), other complementary techniques, namely thermogravimetric analysis and magnetic measurements, were used to determine the eventual valence of chromium.

4. Chromium oxidation state

4.1. TGA analysis

Thermogravimetric analysis showed that upon heating mixture of Bi_2O_3–Cr_2O_3 under air, in stoichiometric amounts for the title compound, an irreversible increase in weight begins at 450–500 °C and reaches at 650 °C a plateau which is observed until 900 °C (Fig. 1). This weight increase can be attributed to the oxidation of Cr^{3+} (from the starting reactants) to Cr^{x+} (in the final compound) and leads to an average valence state $x = +5.83$ for chromium, approaching Cr + VI but with a discrepancy still incompatible with our measurement. To clarify this point, magnetic susceptibility analysis were undertaken.

4.2. Magnetism

Measurement of the magnetization appears the most adapted technique to distinguish between the diamagnetic Cr^{VI}($S = 0$) and paramagnetic Cr^{V}($S = 1/2$) and Cr^{VI} ($S = 1$) ions in the title compound. It has been performed on the $Bi_{31}Cr_5O_{61.5-x}$ prepared powder sample, which appears as a single-phase from XRD analysis. Despite the strong dilution of chromium in the diamagnetic Bi-based lattice, the paramagnetic signal is expected to predominate in the Cr^{IV} or ^{V} hypothesis. In fact this hypothesis is immediately discarded by the negative magnetization measured in the full thermal domain strongly attesting the presence of Cr^{VI} only.

4.3. Back to the structure refinement

According to the +VI valence state of chromium, and considering +III bismuth atoms, the actual formula is then $Bi_{31}Cr_5O_{61.5}$. Some oxygen atoms were then not evidenced with our X-ray experiment.

4.3.1. Oxygen atoms rate determination

As already pointed out, the localisation of extra-oxygen atoms is difficult because of the contrast of bismuth atoms compared to oxygen ones. After Fourier Difference, few supplementary extra peaks were found and considered carefully but were not inserted in the final refinement, since they did not converge to reliable positions. So, even if the final formula is $Bi_{31}Cr_5O_{61.5}$, our single crystal refinement is not showing these extra-oxygen atoms in the structure. This might be an interesting point regarding oxygen mobility properties, indicating some possibly disordered sites. However, to be definitely sure of oxygen location and amount in the structure, a neutron diffraction study might be interesting to manage.

4.3.2. CrO_4 polyhedra treatment

Because of the number of reflexion with low intensity regarded to the small number of reflexion with significant intensity (27,520 reflections and 20,000 with $I < 3\sigma(I)$), CrO_4 tetrahedra were regarded as rigid molecular groups in the structural refinement. This particular strategy allows reducing the number of parameters to be refined (566 parameters without Rigid Body and 486 parameters with) and to adapt to the particular data set. The rigidity of chromate group was determined by a number of common parameters for all the constituting atoms. Each position of the rigid group was defined (and refined) by three swing angles (Φ, χ and ψ) and a translation vector (x_{trans}, y_{trans} and z_{trans}).

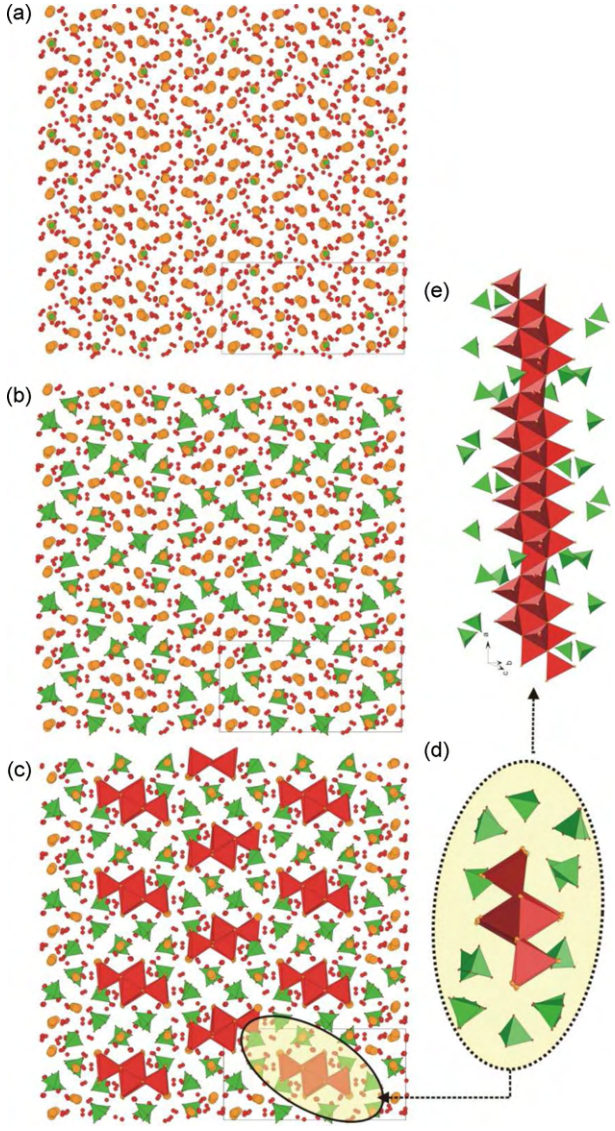

Fig. 2. (a) "Classical" δ-Bi_2O_3 fluorite type structure with some Bi replaced by Cr atoms, (b) CrO_4 tetrahedra configuration, (c) undulated OBi_4 units surrounded by 10 CrO_4 entities and (e) OBi_4 infinite ribbons observed along the perpendicular direction.

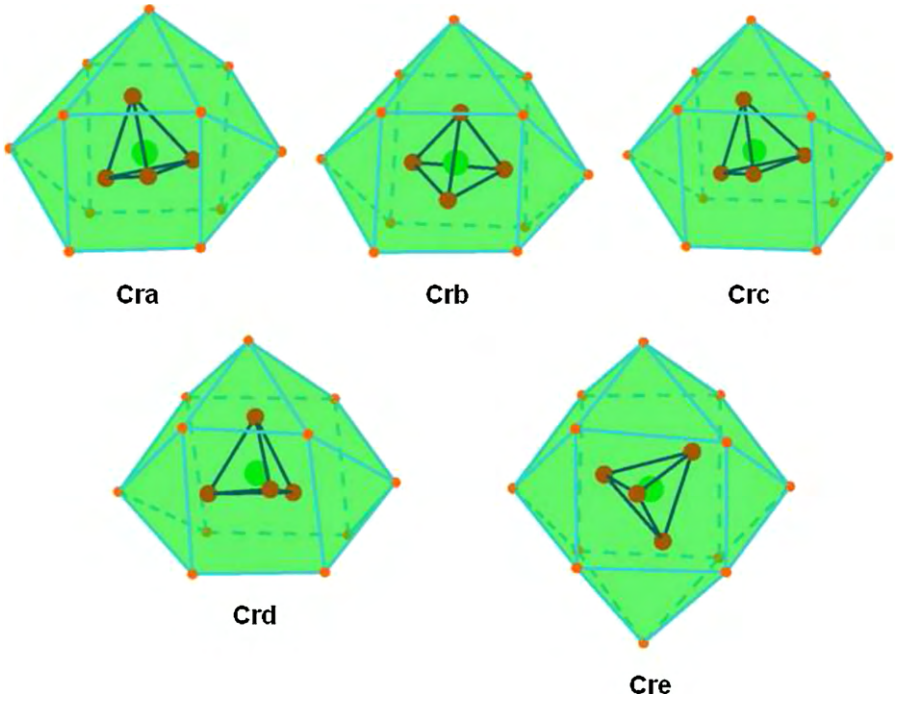

Fig. 3. Local coordination of Cr^{6+} by 11 or 12 Bi atoms forming either a truncated cuboctahedron (Cra to Crd) or a cuboctahedron (Cre).

In these last cycles of refinement, anisotropic displacement were considered for every Bi atoms yielding final $R = 0.0540$ ($R_{all} = 0.1854$) and w$R = 0.0561$ (w$R_{all} = 0.0706$), with a $1/\sigma^2$ weighting scheme.

The crystallographic characteristics, conditions of data collection and various refinement parameters are gathered in Table 1. The atomic coordinates with isotropic and anisotropic thermal parameters and selected bond distances and angles are available in Supplementary materials.

4.4. Structure description

The structure can be describe like a "classical" δ-Bi_2O_3 fluorite type structure, in which some Bi atoms are locally replaced by Cr ones (Fig. 2a), these lasts being in a 4-fold tetrahedral surrounding (CrO_4), Fig. 2b. Looking at the structure along the (1 0 0) axis let appear some ribbons delimited by ten CrO_4 moieties (Fig. 2c and d). If fact, these ribbons are constructed by the associations of undulated OBi_4 anti-tetrahedral units which are alternatively in up and down configuration (Fig. 2e).

Another good way to describe this complex atomic arrangement is to consider the local environment of Cr^{+VI} atoms. In that case, the 5 chromium atoms are at the center of CrO_4 tetrahedra, and in this description, there is no Cr–O–Cr bridging bond. CrO_4 entities are then surrounded by either 11 or 12 Bi^{3+} forming $CrBi_{11}$ truncated cuboctahedra or $CrBi_{12}$ cuboctahedra, respectively (Fig. 3). The various CrO_4 tetrahedra are differently oriented inside the different polyhedra. This description is similar to the one done by Esmaeilzadeh et al. with compounds of the solid solution $Bi_{1-x}Cr_xO_{1.5+1.5x'}$, $0.05 \leq x \leq 0.15$ using a commensurate approximation of the average cubic fluorite structure. In their description, all the chromium atoms are surrounded by 12 bismuth atoms, and consequently are in the center of cuboctahedra. In our compound, only one CrO_4 tetrehedra is in this 12-fold configuration, the four remaining ones lying in $CrBi_{11}$ truncated cuboctahedra. At this stage, one has to remember that the Esmaeilzadeh description is made for an average cubic approximant, while in the present case no approximation was made, implying a 36 times larger cell. Finally, in our structure determination, bismuth atoms are coordinated by between 6 and 8 oxygen atoms making some more or less oxygen deficient BiO_8 cubes, while in Esmaeilzadeh[15] study, bismuth atoms are surrounded by 7 or 8 oxygen atoms forming BiO_7 polyhedra and BiO_8 cubes.

4.5. High temperature X-ray diffraction study

Pure powder sample has been synthesized and characterized by X-ray powder diffraction (Fig. 4). Refined unit cell parameters are: $a = 23.5876(4)$, $b = 11.6401(2)$, $c = 24.3368(4)$ Å and $\beta = 108.06(1)^\circ$.

An X-ray diffraction study versus temperature has also been done in order to check the stability of the phase. Sample was heated from room temperature to 850° and then cooled back to room temperature. The obtained X-ray diagram does not show any unit cell transition, or transformation (Fig. 5). The refinement of unit cell parameters indicates a logical evolution with heating and cooling (Fig. 6). One should note that, contrarily to pure Bi_2O_3, the absence

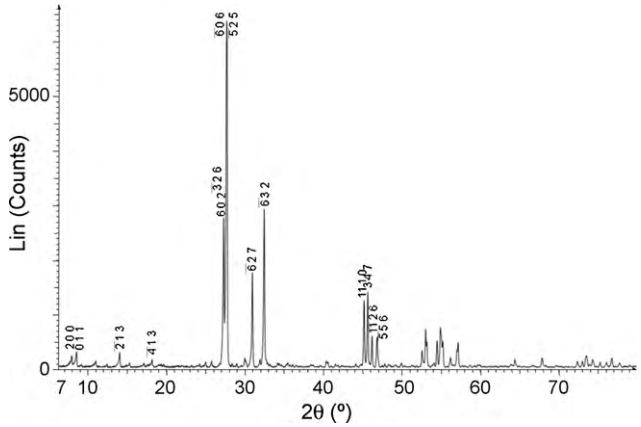

Fig. 4. Indexed X-ray diffraction diagram of the pure $Bi_{31}Cr_5O_{61.5}$ powder sample recorded at room temperature. For clarity reasons, only peaks with highest intensity have been labelled.

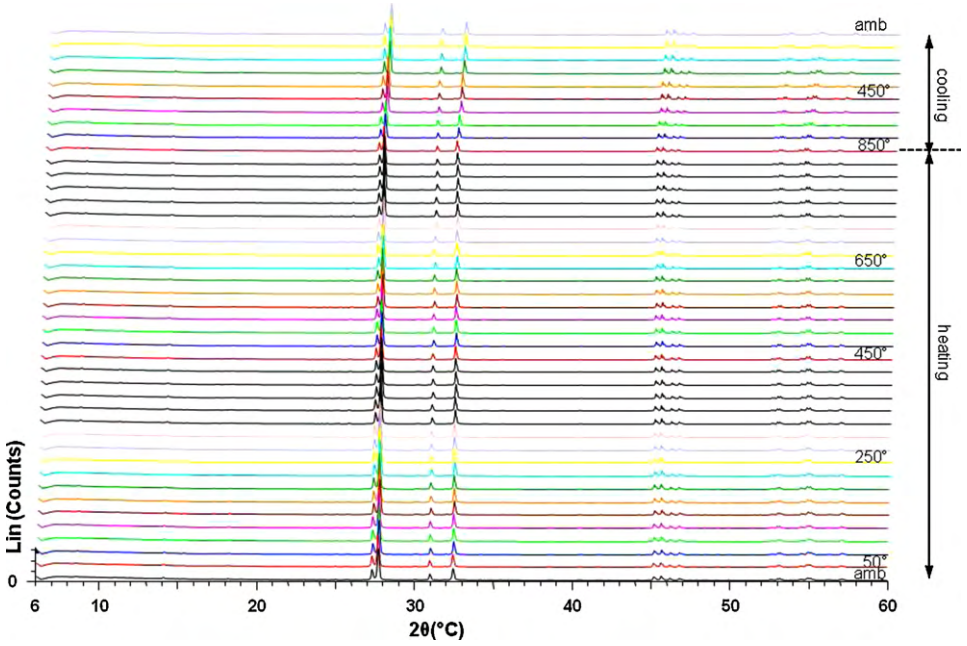

Fig. 5. High-temperature X-ray diffraction data for $Bi_{31}Cr_5O_{61.5}$. Any phase transition is observed during the heating and cooling process.

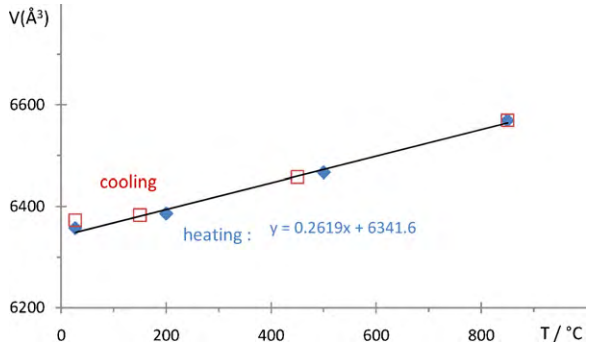

Fig. 6. Cell volume evolution versus temperature for $Bi_{31}Cr_5O_{61.5}$ giving the thermal expansion coefficient.

of phase transition on the whole stability domain is interesting since it prevents any crack formation during a possible thermal cycling on ceramics.

The evolution versus temperature of the cell volume (Fig. 6) and of the different lattice constants drawn using the data of Table 2, allowed the determination of the volume and linear thermal expansion coefficients α: $\alpha_V = 41.3 \times 10^{-6}$, $\alpha_a = 19.4 \times 10^{-6}$, $\alpha_b = 19.5 \times 10^{-6}$, $\alpha_c = 4.7 \times 10^{-6}$ (K^{-1}). Note that, the thermal expansion of the material which appears isotropic in the *ab* plane is significantly lower in the *c* axis direction. To complete this study, some dilatometry measurements were undertaken.

Table 2
Refined unit cell parameters depending of temperature.

Temperature	*a*(Å)	*b*(Å)	*c*(Å)	*β*(°)	*V*(Å³)
Amb	23.585(5)	11.642(4)	24.345(6)	108.00(2)	6357.4
200°	23.648(5)	11.686(4)	24.337(6)	108.28(2)	6386.1
500°	23.781(5)	11.744(4)	24.397(6)	108.36(2)	6466.8
850°	23.960(5)	11.832(4)	24.428(6)	108.45(2)	6569.2
450°	23.768(5)	11.733(4)	24.391(6)	108.30(2)	6457.9
150°	23.633(5)	11.675(4)	24.342(6)	108.12(2)	6383.2
Amb	23.590(5)	11.680(4)	24.325(6)	108.02(2)	6373.5

4.6. Dilatometry

Fig. 7 presents the thickness evolution of a pellet of material (diameter: 5 mm; thickness: 4 mm). As previously indicated by HTXRD, this evolution did not reveal any phase transition in the material during the thermal cycle. The lower part of the figure shows the quasi-linearity of the thickness modification in the 200–500 °C temperature range and displays the equation of this considered linear evolution. From this equation and the thickness value, the linear thermal expansion coefficient of the thickness could be evaluated: $\alpha_{th.} = 1.4 \times 10^{-6}$ (K^{-1}). The comparison of this

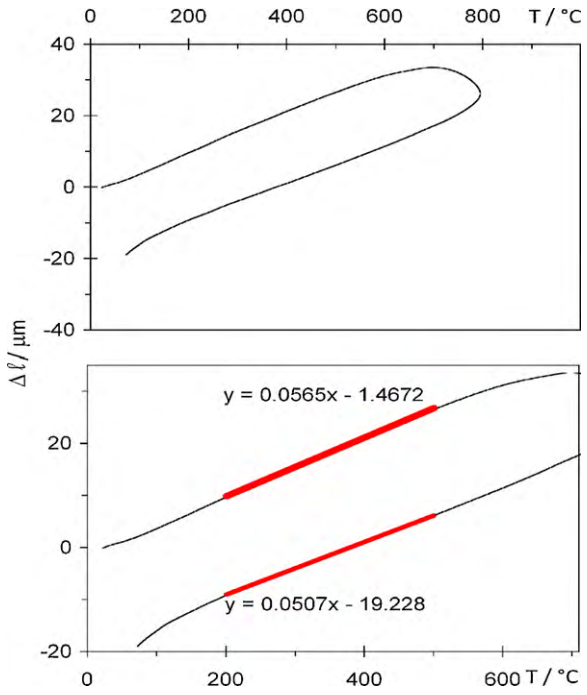

Fig. 7. Dilatometry analysis of $Bi_{31}Cr_5O_{61.5}$ pellet showing a quasi linear evolution of the thickness between 200 and 500 °C.

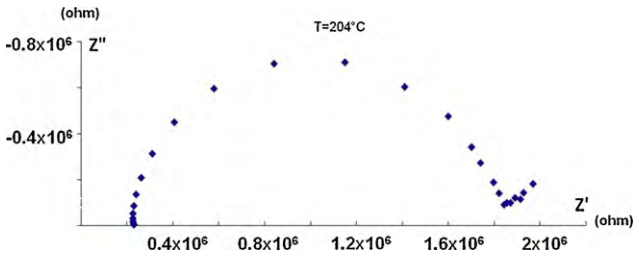

Fig. 8. Impedance spectrum recorded at 204 °C for $Bi_{31}Cr_5O_{61.5}$ pellet.

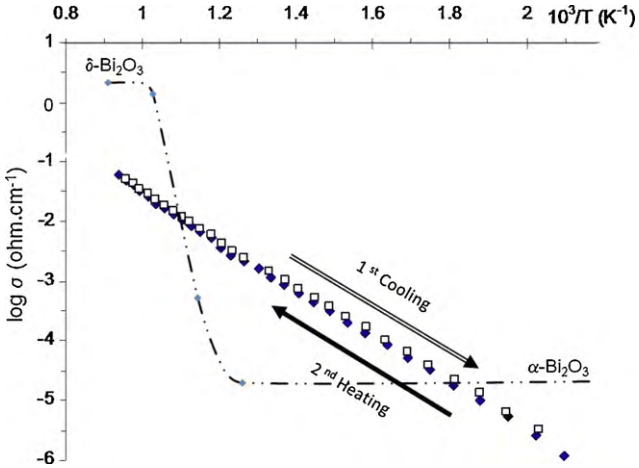

Fig. 9. Heating–cooling conductivity Arrhenius plot for $Bi_{31}Cr_5O_{61.5}$ pellet compared with Bi_2O_3.

value to the values of parameter thermal expansion coefficients determined from X-ray data, seems indicate that the material crystallite are strongly oriented in the pellet such as a and b axis are parallel to the pellet surfaces and c axis almost perpendicular to these surfaces.

4.7. Conductivity

The measurements realized during the first heating run which are generally erroneous because of the evolution of the sample–electrodes–cell interfaces, cannot be trusted. The results corresponding to the first cooling run were reproducible during the following thermal cycles. These measurements were used and we present the results corresponding to a pellet with the following dimensions: diameter 4.9 mm and thickness 3.46 mm. Fig. 8 presents the impedance diagram obtained for material heated at 204 °C. One circle only characterizes the response of the bulk and that of the grain boundaries of the so-sintered material, in the high frequency range. The beginning of the circle which characterizes the electrode response is also observed in the low frequency range. Fig. 9 presents the Arrhenius plot corresponding to the second thermal cycle. Only one linear domain is observed within the investigated temperature domain, in agreement with the absence of any phase transition, claimed from the high-temperature X-ray investigation.

5. Conclusion

The complex structure of the new $Bi_{31}Cr_5O_{61.5}$ has been determined. The phase stability of the compound with temperature and the preliminary conductivity measurements are encouraging and make it a potential candidate as an electrode material for SOFC. The next step of this study might be to test its electronic conductivity, and to undertake neutrons diffraction measurement to clarify the oxygen mobility.

Acknowledgements

The Fonds Européen de Développement Régional (FEDER), CNRS, Région Nord Pas-de-Palais, and Ministère de l'Education Nationale de l'Enseignement Supérieur et de la Recherche are acknowledged for funding of X-ray diffractometers. Nora Djelal is thanked for its precious technical help in synthesis and SEM analysis. The SEM facility in Lille (France) is supported by the Conseil Regional du Nord-Pas de Calais, and the European Regional Development Fund (ERDF). Olivier Mentré is thanked for magnetic study.

Appendix A. Supplementary data

Supplementary data associated with this article can be found, in the online version, at doi:10.1016/j.jpowsour.2010.05.013.

References

[1] D.J. Boivin, G. Mairesse, Chem. Mater. 10 (1998) 2870.
[2] M. Drache, P. Roussel, J.P. Wignacourt, Chem. Rev. 107 (2007) 80.
[3] T. Takahashi, H. Iwahara, T. Arao, J. Appl. Electrochem. 5 (1975) 187.
[4] T. Takahashi, H. Iwahara, T. Arao, J. Appl. Electrochem. 5 (1975) 197.
[5] P. Conflant, C. Follet-Houttemane, M. Drache, J. Mater. Chem. 1 (1991) 649.
[6] M. Omari, M. Drache, P. Conflant, J.C. Boivin, Solid State Ionics 40/41 (1990) 929.
[7] N. Portefaix, P. Conflant, J.C. Boivin, J.P. Wignacourt, M. Drache, JSSC 134 (1997) 219.
[8] O. Labidi, P. Roussel, M. Huvé, M. Drache, P. Conflant, J.P. Wignacourt, JSSC 178 (2005) 2247–2255.
[9] H.A. Harwind, Z. Anorg, Allg. Chem. 444 (1978) 151.
[10] T.E. Crumpton, M.G. Francesconi, C. Greaves, JSSC 175 (2003) 197.
[11] M. Valldor, S. Esmaeilzadeh, C. Pay-Gomez, J. Grins, JSSC 152 (2000) 573.
[12] N. Kumada, T. Takei, N. Kinomura, G. Wallez, JSSC 179 (2006) 793.
[13] Y.H. Liu, J.B. Li, J.K. Liang, J. Luo, L.N. Ji, J.Y. Zhang, G.H. Rao, Mater. Chem. Phys. 112 (2008) 239.
[14] O. Labidi, J.P. Wignacourt, P. Roussel, M. Drache, P. Conflant, H. Steinfink, Solid State Sci. 6 (2004) 783–790.
[15] J. Grins, S. Esmaeilzadeh, S. Hull, JSSC 163 (2002) 144.
[16] S. Esmaeilzadeh, S. Lundgren, U. Halenius, J. Grins, JSSC 156 (2001) 168.
[17] L. Palatinus, G. Chapuis, J. Appl. Cryst. 40 (2007) 786–790.
[18] V. Petricek, M. Dusek, L. Palatinus, The Crystallographic Computing System, Institute of Physics, Praha, Czech Republic, 2006.